



UNIVERSITY OF LEEDS

This is a repository copy of *Determination of the atmospheric lifetime and global warming potential of sulphur hexafluoride using a three-dimensional model*.

White Rose Research Online URL for this paper:  
<http://eprints.whiterose.ac.uk/111136/>

Version: Published Version

---

**Article:**

Kovács, T, Feng, W [orcid.org/0000-0002-9907-9120](https://orcid.org/0000-0002-9907-9120), Totterdill, A et al. (10 more authors) (2016) Determination of the atmospheric lifetime and global warming potential of sulphur hexafluoride using a three-dimensional model. Atmospheric Chemistry and Physics Discussions. ISSN 1680-7367

<https://doi.org/10.5194/acp-2016-671>

---

**Reuse**

This article is distributed under the terms of the Creative Commons Attribution (CC BY) licence. This licence allows you to distribute, remix, tweak, and build upon the work, even commercially, as long as you credit the authors for the original work. More information and the full terms of the licence here:  
<https://creativecommons.org/licenses/>

**Takedown**

If you consider content in White Rose Research Online to be in breach of UK law, please notify us by emailing [eprints@whiterose.ac.uk](mailto:eprints@whiterose.ac.uk) including the URL of the record and the reason for the withdrawal request.



[eprints@whiterose.ac.uk](mailto:eprints@whiterose.ac.uk)  
<https://eprints.whiterose.ac.uk/>



1           **Determination of the atmospheric lifetime and global**  
2           **warming potential of sulphur hexafluoride using a three-**  
3           **dimensional model**

4           Tamás Kovács<sup>1</sup>, Wuhu Feng<sup>1,2</sup>, Anna Totterdill<sup>1</sup>, John M.C. Plane<sup>1</sup>, Sandip Dhomse<sup>2</sup>,  
5           Juan Carlos Gómez-Martín<sup>1</sup>, Gabriele P. Stiller<sup>3</sup>, Florian J. Haenel<sup>3</sup>, Christopher Smith<sup>4</sup>,  
6           Piers M. Forster<sup>2</sup>, Rolando R. García<sup>5</sup>, Daniel R. Marsh<sup>5</sup> and Martyn P. Chipperfield<sup>2\*</sup>

7           <sup>1</sup>School of Chemistry, University of Leeds, Leeds LS2 9JT, UK.

8           <sup>2</sup>NCAS, School of Earth and Environment, University of Leeds, Leeds LS2 9JT, UK.

9           <sup>3</sup>Karlsruhe Institute of Technology, IMK-ASF, PO BOX 3640, 76021 Karlsruhe, Germany.

10          <sup>4</sup>Energy Research Institute, School of Chemical and Process Engineering, University of Leeds,  
11          Leeds LS2 9JT, UK.

12          <sup>5</sup>National Center for Atmospheric Research (NCAR), Boulder, Colorado, USA.

13          \*Correspondence to: Martyn Chipperfield (M.Chipperfield@leeds.ac.uk)

14          **Abstract.** We have used the Whole Atmosphere Community Climate Model (WACCM), with  
15          an updated treatment of loss processes, to determine the atmospheric lifetime of SF<sub>6</sub>. The model  
16          includes the following SF<sub>6</sub> removal processes: photolysis, electron attachment and reaction  
17          with mesospheric metal atoms. The Sodankylä Ion Chemistry (SIC) model is incorporated into  
18          the standard version of WACCM to produce a new version with a detailed *D* region ion  
19          chemistry with cluster ions and negative ions. This is used to determine a latitude- and altitude-  
20          dependent scaling factor for the electron density in the standard WACCM in order to carry out  
21          multi-year SF<sub>6</sub> simulations. The model gives a mean SF<sub>6</sub> lifetime over a 11-year solar cycle ( $\tau$ )  
22          of 1278 years (with a range from 1120 to 1475 years), which is much shorter than the currently  
23          widely used value of 3200 years, due to the larger contribution (97.4%) of the modelled  
24          electron density to the total atmospheric loss. The loss of SF<sub>6</sub> by reaction with mesospheric  
25          metal atoms (Na and K) is far too slow to affect the lifetime. We investigate how this shorter  
26          atmospheric lifetime impacts the use of SF<sub>6</sub> to derive stratospheric age-of-air. The age-of-air  
27          derived from this shorter lifetime SF<sub>6</sub> tracer is longer by 9% in polar latitudes at 20 km  
28          compared to a passive SF<sub>6</sub> tracer. We also present laboratory measurements of the infrared  
29          spectrum of SF<sub>6</sub> and find good agreement with previous studies. We calculate the resulting  
30          radiative forcings and efficiencies to be, on average, very similar to those reported previously.  
31          Our values for the 20, 100 and 500-year global warming potentials are 18,000, 23,800 and  
32          31,300, respectively.



### 33 **1 Introduction**

34 Sulphur hexafluoride (SF<sub>6</sub>) is an anthropogenic greenhouse gas which is mainly used as an  
35 electrical insulator, with other applications as a quasi-inert gas. Although its main sources are  
36 in the Northern Hemisphere, its atmospheric abundance is increasing globally in response to  
37 these emissions and its long atmospheric lifetime. SF<sub>6</sub> is characterised by large absorption  
38 cross-sections for terrestrial infrared radiation such that the presently increasing SF<sub>6</sub> abundance  
39 will contribute a positive radiative forcing over many centuries. The important known removal  
40 sources are electron attachment and photolysis. Recently, we have also measured bimolecular  
41 rate constants for the reaction of SF<sub>6</sub> with mesospheric metals (Totterdill *et al.*, 2015).

42 Harnisch and Eisenhauer (1998) reported that SF<sub>6</sub> is naturally present in fluorites, and out-  
43 gassing from these materials leads to a natural background atmospheric abundance of 0.01  
44 pptv. However, at present the anthropogenic emissions of SF<sub>6</sub> exceed the natural ones by a  
45 factor of 1000 or more and are responsible for the rapid increase in its atmospheric abundance.  
46 Surface measurements show that SF<sub>6</sub> increased by about 7%/year during the 1980s and 1990s  
47 (Geller *et al.*, 1997; Maiss and Brenninkmeijer, 1998).

48 SF<sub>6</sub> provides a useful tracer of atmospheric transport in both the troposphere and stratosphere.  
49 Rates for transport of pollutants into, within, and out of the stratosphere are important  
50 parameters that regulate stratospheric composition. The basic characteristics of the  
51 stratospheric Brewer-Dobson (B-D) circulation are known from observations of trace gases  
52 such as SF<sub>6</sub>: air enters the stratosphere at the tropical tropopause, rises at tropical latitudes, and  
53 descends at middle and high latitudes to return to the troposphere. Understanding the rate of  
54 this transport on a global scale is crucial in order to predict the response of stratospheric ozone  
55 to climatic or chemical change. SF<sub>6</sub> is essentially inert in the troposphere to middle stratosphere  
56 and is removed by electron attachment and photolysis in the upper stratosphere and mesosphere  
57 (Ravishankara *et al.*, 1993). This tracer therefore provides an ideal probe of transport on  
58 timescales of importance in the stratospheric circulation and quantitative information on mean  
59 air mass age for the lower and middle stratosphere.

60 The mean age-of-air (AoA) is the interval between the time when the volume mixing ratio of  
61 a linearly increasing atmospheric tracer reaches a certain value at a given location in the  
62 stratosphere and an earlier time when this mixing ratio was reached at a reference location.  
63 Mean AoA is expressed as (Hall and Plumb, 1994; Waugh and Hall, 2002)



$$64 \quad \text{AoA} = t(\chi, l, z) - t(\chi, l_0, z_0) \quad (E1)$$

65 where  $t$  is time,  $\chi$  is the volume mixing ratio,  $l$  and  $z$  are latitude and altitude, and the 0 subscripts  
66 denote the reference latitude and altitude which are chosen to be the upper tropical troposphere  
67 (latitude = 1°N, altitude = 13.9 km). In principle the trend of AoA can be used to diagnose  
68 changes in the strength of Brewer-Dobson circulation (BDC); in practice, however, it is very  
69 difficult to obtain unambiguous results on trends from this or any other trace gas (Garcia *et al.*,  
70 2011). Ideally, AoA should be determined experimentally using a tracer with very small (or  
71 zero) chemical sink in the stratosphere or mesosphere. Otherwise, a correction must be applied  
72 to account for this loss. A correction would also be necessary for any non-linear tropospheric  
73 growth. However, for the period considered for diagnosing age-of-air in this paper (2002-2007)  
74 the growth of SF<sub>6</sub> is approximately linear, so we can reasonably neglect such a correction for  
75 SF<sub>6</sub>-derived AoA (Hall and Plumb, 1994).

76 Ravishankara *et al.* (1993) reported the atmospheric lifetime of SF<sub>6</sub> to be 3200 years by  
77 considering electron attachment and vacuum ultraviolet (VUV) photolysis. They also studied  
78 the loss of SF<sub>6</sub> by reaction with O(<sup>1</sup>D) but found the rate too slow to be important. They  
79 deduced that electron attachment was the dominant loss process and quantified this process  
80 using a 2-D model, wherein they assumed that all SF<sub>6</sub> molecules are destroyed after attachment  
81 of an electron (with a rate constant of 10<sup>-9</sup> cm<sup>3</sup> molecule<sup>-1</sup> s<sup>-1</sup>). They therefore argued that their  
82 lifetime of 3200 years could be a lower limit, but clearly this result depends on the accuracy of  
83 the 2-D electron density, which was calculated using only photochemistry. Morris *et al.* (1995)  
84 subsequently extended the work of Ravishankara *et al.* (1993) by including an ion chemistry  
85 module in the same 2-D model. They also made other assumptions to maximise the impact of  
86 electron attachment on SF<sub>6</sub> loss and derived a lifetime as low as 800 years (which could be  
87 further sporadically decreased by large solar proton events). Using a 3-D middle atmosphere  
88 model, Reddman *et al.* (2001) estimated the lifetime to be 472 years when SF<sub>6</sub> is irreversibly  
89 destroyed purely by direct electron attachment and to be 9379 years when SF<sub>6</sub> loss is assumed  
90 to occur only via indirect loss (via the formation of SF<sub>6</sub><sup>-</sup>) and ionization via the reactions with  
91 O<sub>2</sub><sup>+</sup> and N<sub>2</sub><sup>+</sup>. They concluded that the estimated lifetime depends strongly on the electron  
92 attachment mechanism, because the efficiency of this process as a permanent removal process  
93 of SF<sub>6</sub> depends on the competition between reaction of SF<sub>6</sub><sup>-</sup> with H and HCl, and  
94 photodetachment and reaction with O and O<sub>3</sub>. Here we extend on the above studies and  
95 investigate the SF<sub>6</sub> lifetime using a state-of-the-art 3-D chemistry climate model with a domain



96 from the surface to 140 km. Our modelled electron density is based on results of a detailed ion  
97 chemistry model and we use a detailed methodology for treating the atmospheric background  
98 electrons, which is based on Troe's formalism (Troe *et al.*, 2007a,b; Viggiano *et al.*, 2007).

99 In addition to determining the SF<sub>6</sub> lifetime, in this study we report new measurements of the  
100 infrared absorption cross-sections for SF<sub>6</sub> and input these into a line-by-line radiative transfer  
101 model in order to obtain radiative forcings and efficiencies. These values are then used to  
102 determine more accurate values of global warming potentials (GWPs) based on their cloudy  
103 sky adjusted radiative efficiencies. GWP is the metric used by the World Meteorological  
104 Organisation (WMO) and Intergovernmental Panel on Climate Change (IPCC) to compare the  
105 potency of a greenhouse gas relative to an equivalent emission of CO<sub>2</sub> over a set time period.  
106 The definitions of these radiative terms are discussed in detail in our recent publication  
107 Totterdill *et al.* (2016).

## 108 **2 Methodology**

### 109 **2.1 WACCM 3D model**

110 To simulate atmospheric SF<sub>6</sub> we have used the Whole Atmosphere Community Climate Model  
111 (WACCM). Here we use WACCM 4 (Marsh *et al.*, 2013), which is part of the NCAR  
112 Community Earth System Model (CESM; Lamarque *et al.*, 2012), configured to have 88  
113 pressure levels from the surface to the lower thermosphere ( $5.96 \times 10^{-6}$  Pa, 140 km) and a  
114 horizontal resolution of  $1.9^\circ \times 2.5^\circ$  (latitude  $\times$  longitude). The model contains a detailed  
115 treatment of middle atmosphere chemistry including interactive treatments of Na and K (Plane  
116 *et al.*, 2015). We use the specified dynamics (SD) version of the model to allow comparison  
117 with observations (see Garcia *et al.*, (2014) for details). The SF<sub>6</sub> surface emission flux and  
118 initial global vertical profiles were taken from a CCMI (Chemistry Climate Model Initiative)  
119 simulation using the same version of SD-WACCM with the same nudging analyses (D.  
120 Kinnison, personal communication, 2013).

121 Lyman- $\alpha$  photolysis is the only SF<sub>6</sub> loss reaction in the standard version of WACCM and in  
122 this work we have added the additional processes given in **Table 1**. The rate constants for the  
123 SF<sub>6</sub> + metal reactions have been measured in our laboratory for mesospheric conditions  
124 (Totterdill *et al.*, 2015); here we use the experimental values for the reactions with Na and K.  
125 For the photolysis of SF<sub>6</sub> we used the standard WACCM methodology but with the updated  
126 Lyman- $\alpha$  cross section from our laboratory of  $1.37 \times 10^{-18}$  cm<sup>2</sup> molecule<sup>-1</sup> (Totterdill *et al.*,  
127 2015). The WACCM Lyman- $\alpha$  flux is taken from Chabrilat and Kockarts (1997).



128 Electron attachment to SF<sub>6</sub> plays a major role in its atmospheric removal and so both  
 129 dissociative and non-dissociative attachment are considered in this study. The detailed method  
 130 is described in a recent paper (Totterdill *et al.*, 2015) and here only a brief summary is given.  
 131 The removal process by the attachment of low energy electrons to SF<sub>6</sub> can be described using  
 132 Troe's theory (Troe *et al.*, 2007a,b; Viggiano *et al.*, 2007). In the middle and lower mesosphere,  
 133 electrons are mostly attached to neutral species in the form of anions. However, above 80 km  
 134 the concentration of free electrons increases and the direct electron attachment to SF<sub>6</sub> becomes  
 135 more likely. This can happen either by associative attachment forming the SF<sub>6</sub><sup>-</sup> anion which  
 136 can then undergo chemical reactions with H, O, O<sub>3</sub> and HCl, or by dissociative attachment  
 137 forming the SF<sub>5</sub><sup>-</sup> anion fragment. The probability  $\beta$  of dissociative attachment when an electron  
 138 is captured by SF<sub>6</sub> is given by

$$139 \quad \beta(p, T) = \frac{k_{dis}}{k_{at} + k_{dis}} \quad (E2)$$

140 where  $k_{dis}$  is the rate constant for dissociative attachment and  $k_{at}$  is the rate constant for  
 141 associative attachment.  $\beta$  can be expressed as

$$142 \quad \beta(p, T) = \exp(-4587T + 7.74) \times 10^{\left[4.362 - 0.582 \log_{10}(p/Torr) - 0.0203 \left(\log_{10}\left(\frac{p}{Torr}\right)\right)^2\right] / 5.26 \times 10^{-4}} \quad (E3)$$

144 where  $T$  is the temperature in K and  $p$  is the pressure in Torr (Totterdill *et al.*, 2015).

145 We include both associative and dissociative electron attachment using WACCM-predicted  
 146 electron concentrations (see **Table 1**). Note that the SF<sub>6</sub><sup>-</sup> anion is not modelled directly. Instead  
 147 the SF<sub>6</sub> attachment loss rate is calculated by multiplying  $k_{at}$  by the probability of permanent  
 148 destruction of the resulting SF<sub>6</sub><sup>-</sup> (reactions of SF<sub>6</sub><sup>-</sup> with H and HCl) to the sum of these reactions  
 149 and processes which recycle SF<sub>6</sub><sup>-</sup> to SF<sub>6</sub> (reactions with O and O<sub>3</sub>, and photodetachment)  
 150 (Morris *et al.*, 1995).

151 In order to use a realistic electron concentration, the role of negative ions in the  $D$  region must  
 152 be considered. Therefore, a scaling factor was introduced that converts the standard WACCM  
 153 electron concentrations, which are calculated from charge balance with the five major positive  
 154  $E$  region ions (N<sup>+</sup>, N<sub>2</sub><sup>+</sup>, O<sup>+</sup>, O<sub>2</sub><sup>+</sup> and NO<sup>+</sup>), to more realistic electron concentrations. We have  
 155 recently incorporated the Sodankylä Ion Chemistry (SIC) model into the standard version of  
 156 WACCM to produce a new version (WACCM-SIC) containing a detailed  $D$  region ion



157 chemistry with cluster ions and negative ions (Kovács *et al.*, 2016). The mesospheric positive  
158 and negative ions in WACCM-SIC are listed in **Table 2**. The electron scaling factor in each  
159 grid box of WACCM was then defined as the annually averaged ratio of  $[e]_{\text{WACCM-SIC}}/[e]_{\text{WACCM}}$   
160 for the year 2013, where  $[e]_{\text{WACCM-SIC}}$  is the electron density calculated from WACCM-SIC  
161 and  $[e]_{\text{WACCM}}$  from the standard WACCM.

162 The scaling factor, which varies with altitude and latitude, is shown in **Figure 1** (bottom panel)  
163 together with the electron densities from the standard WACCM (top panel) and WACCM-SIC  
164 (middle panel) models. The annually averaged electron concentration in the WACCM-SIC  
165 model is significantly smaller in the lower and middle mesosphere than in the standard  
166 WACCM, which is expected because of negative ion formation. Note that in the upper  
167 mesosphere (70 - 80 km) the electron density in WACCM-SIC is larger than WACCM. This  
168 results from the inclusion of medium energy electrons (MEE) (electrons with energy between  
169 30 keV and 2MeV) in WACCM-SIC. **Figure 2** shows the effect of MEE by comparing  
170 WACCM-SIC runs with and without this source of ionization in the upper mesosphere  
171 included. To describe the effect of ionization, WACCM-SIC uses ionization rates ( $I$ ) as a  
172 function of time and pressure which were calculated from the spectra based on the proton  
173 energy-range measurements in standard air as described by Verronen *et al.* (2005). According  
174 to Figure 3 of Meredith *et al.* (2015), the annually averaged medium energy electron flux for  
175 2013 approximately corresponds to the long-term, 20-year average. This allows us to assume  
176 that the annually averaged electron density of 2013 from WACCM-SIC can be used to scale  
177 the long-term simulations using the standard WACCM aimed at determining the atmospheric  
178 lifetime of SF<sub>6</sub>.

179 The WACCM simulation included five different SF<sub>6</sub> tracers in order to quantify the importance  
180 of different loss processes. All of these tracers used the same emissions but differed in their  
181 treatment of SF<sub>6</sub> loss reactions. One SF<sub>6</sub> tracer included no atmospheric loss (i.e. a passive  
182 tracer). Three tracers included one of the following loss processes for SF<sub>6</sub>: (i) reaction with  
183 mesospheric metals (Na, K), (ii) electron attachment, and (iii) UV photolysis. Finally, one ‘total  
184 reactive’ SF<sub>6</sub> tracer included all three loss processes. This total reactive tracer should be the  
185 most realistic and was used in the radiative forcing calculations. WACCM was run for the  
186 period 1990-2007, and the first five years were treated as spin-up. For the analysis the monthly  
187 mean model outputs were saved and later globally averaged for the lifetime calculations.

188



## 189 2.2 Infrared absorption spectrum and radiative forcing

190 Previous quantitative infrared absorption spectra of SF<sub>6</sub> have been compared in Hodnebrog *et*  
191 *al.* (2013) (their Table 12). There are differences of ~10% between existing integrated cross-  
192 section estimates, and the measurements cover different spectral ranges. We therefore  
193 performed a more complete set of measurements over a wider spectral range, in order to reduce  
194 uncertainty in the absorption spectrum and hence the radiative efficiency of SF<sub>6</sub>. Measurements  
195 were taken using an experimental configuration consisting of a Bruker Fourier transform  
196 spectrometer (Model IFS/ 66), which was fitted with a mid-infrared (MIR) source used to  
197 generate radiation which passed through an evacuable gas cell with optical path length 15.9  
198 cm. The cell was fitted with KBr windows, which allow excellent transmission between 400  
199 and 40,000 cm<sup>-1</sup>. The choice of source and window were selected so as to admit radiation across  
200 the mid IR range where bands of interest are known to occur. Room temperature (296 ± 2 K)  
201 measurements were carried out between 400 and 2000 cm<sup>-1</sup> at a spectral resolution of 0.1 cm<sup>-1</sup>  
202 and compiled from the averaged total of 128 scans to 32 background scans at a scanner velocity  
203 of 1.6 kHz. Gas mixtures were made using between 8 and 675 Torr of SF<sub>6</sub> diluted up to an  
204 atmosphere using N<sub>2</sub>, according to the method described in Totterdill *et al.* (2016).

205 Radiative forcing calculations were made using the Reference Forward Model (RFM) (Dudhia,  
206 2013) which is a line-by-line radiative transfer model based on the previous GENLN2 model  
207 (Edwards, 1987). Results obtained from this model were validated against the DISORT  
208 radiative transfer solver (Stamnes *et al.*, 2000) included within the libRadtran (Library for  
209 Radiative Transfer) package (Mayer and Kylling, 2005). A full description of these models and  
210 parameters used alongside discussion of treatment of clouds and model comparison is also  
211 given in Totterdill *et al.* (2016).

## 212 3 Results

### 213 3.1 Global distributions of SF<sub>6</sub> from WACCM simulations

214 **Figure 3** shows typical zonal mean profiles of the WACCM SF<sub>6</sub> tracers in the north and south  
215 polar regions for different seasons, compared to MIPAS observations for the year 2007 (Haenel  
216 *et al.*, 2015). Although the MIPAS SF<sub>6</sub> data provides much more coverage horizontally and  
217 vertically compared to in situ aircraft and balloon data, it has only been validated up to 35 km  
218 (Stiller *et al.*, 2008). At higher altitudes validation is not possible due to the lack of suitable  
219 reference data. Details of the validation of the MIPAS data version used here (V5h\_SF6\_20  
220 for the full resolution product from 2004 and earlier; V5r\_SF6\_222 and V5r\_SF6\_223 for the





221 reduced resolution period of 2005 and later) can be found in Haenel *et al.* (2015), including  
222 Figure S-2 of their supplementary material. The WACCM passive SF<sub>6</sub> tracer has a mixing ratio  
223 profile that is fairly constant with altitude until around 70 km, after which it decreases.  
224 Comparison of the tracers that include loss processes show that removal of SF<sub>6</sub> is dominated  
225 by electron attachment, with a small contribution direct from photolysis. The mesospheric  
226 metals make a negligible contribution because the Na and K layers occur in the upper  
227 mesosphere above 80 km (with peaks around 90 km), and the concentrations of these metal  
228 atoms are too low. As is clear from **Figure 3**, the model simulation and satellite observations  
229 agree within the atmospheric variability, which becomes relatively large above 30 km  
230 especially at high latitudes, although the model is systematically larger than the observations  
231 above 20 km. The time variation of modelled SF<sub>6</sub> shown in **Figure 4** corresponds to an  
232 emission rate (slope) of  $6.5 \times 10^{-3}$  Tg/year, i.e. a 0.29 pptv/year increase in global mean volume  
233 mixing ratio, and a volume mixing ratio of 6.4 pptv by the end of 2007.

234 **Figure 5** shows the zonal mean annual mean SF<sub>6</sub> distribution from the five WACCM tracers  
235 and MIPAS observations for 2007. **Figure 5a** (and **Figure 3**) shows that there is a rapid  
236 decrease in SF<sub>6</sub> above 75 km even for the inert tracer. This can be explained by diffusive  
237 separation, which becomes pronounced in the upper mesosphere because SF<sub>6</sub> is a relatively  
238 heavy molecule compared to the mean molecular mass of air molecules (cf. Garcia *et al.* (2014),  
239 where similar behaviour is seen for CO<sub>2</sub>, another relatively heavy molecule). Panels (a)-(c) of  
240 the figure all show SF<sub>6</sub> decreasing above ~80 km, and panels (a) and (c) are almost identical,  
241 while in panel (b) the decrease begins a little lower. This is all consistent with the notion that  
242 metals do not affect SF<sub>6</sub> and photolysis contributes only slightly. The fact that diffusive  
243 separation prevents SF<sub>6</sub> from reaching altitudes where photolysis is faster must be contributing  
244 to the very long lifetime found when photolysis is the only loss considered. By contrast, in  
245 **Figure 5d** SF<sub>6</sub> decreases rapidly above 70 km, which is related to the fact that loss via electron  
246 attachment is important at these lower altitudes. Thus, in this case, SF<sub>6</sub> loss occurs below the  
247 altitudes where diffusive separation is important (and where air density is higher), which makes  
248 it a much more effective loss mechanism. The WACCM SF<sub>6</sub> tracer that includes all loss  
249 processes (**Figure 5e**) has a very similar distribution to that which only treats loss due to  
250 electron attachment (**Figure 5d**), which emphasises how this process dominates SF<sub>6</sub> loss in the  
251 model. This model tracer can be compared to the MIPAS observations in **Figure 5f**, which  
252 shows that WACCM agrees reasonably well with the measurements in the lower stratosphere  
253 (note the smaller altitude range in panels (e) and (f) of **Figure 5**). Finally, it is also clear that



254 WACCM SF<sub>6</sub>, even with all losses considered, decreases with altitude much more slowly at all  
255 latitudes than MIPAS SF<sub>6</sub>. This could indicate a problem with the model's meridional transport.  
256 However, a too-fast BDC would tend to produce low levels of SF<sub>6</sub> at middle and high latitudes  
257 in the descending branch, which does not seem to be the case. Therefore, at least two other  
258 possible scenarios could be responsible for the discrepancy: SF<sub>6</sub> loss in WACCM is still  
259 somewhat underestimated despite the inclusion of the electron attachment, or MIPAS SF<sub>6</sub> is  
260 biased low above ~20 km.

### 261 3.2 Atmospheric lifetime

262 The atmospheric lifetime is defined as the ratio of the atmospheric burden to the atmospheric  
263 loss rate. This definition was used to calculate annual mean lifetime values from the WACCM  
264 output containing the individual rates for the different loss processes. During the simulation  
265 the total atmospheric burden of SF<sub>6</sub> increased linearly as expected (see **Figure 4**) from  $3.4 \times 10^{32}$   
266 molecules with an annual increment of  $2.3 \times 10^{31}$  molecules/year. **Figure 6** shows the variation  
267 in SF<sub>6</sub> lifetime from 1995 to 2007, corresponding to a full solar cycle (the solar minima  
268 occurred in May 1996 and January 2008). The figure demonstrates that the lifetime has a strong  
269 dependence on solar activity, being anti-correlated with the solar radio flux at 10.7 cm (2800  
270 MHz) (Tapping, 2013) which ranges over  $(72 - 183) \times 10^{-22} \text{ W m}^{-2} \text{ Hz}^{-1}$ , with an average value  
271 of  $90.3 \times 10^{-22} \text{ W m}^{-2} \text{ Hz}^{-1}$ . The mean SF<sub>6</sub> lifetime and range over the same solar cycle period  $\tau$   
272 = 1278 years, with a range from 1120 to 1475 years. The annual averaged electron number  
273 density in the polar regions is also plotted in **Figure 6**; as expected, it is correlated with the  
274 10.7 cm radio emission (Tapping, 2013).

275 As noted in the Introduction, the SF<sub>6</sub> lifetime has been reported to be 3200 years by  
276 Ravishankara *et al.*, (1993). For this they used a total electron attachment rate constant of  $k_{\text{EA}}$   
277 =  $10^{-9} \text{ cm}^3 \text{ s}^{-1}$ . In Morris *et al.* (1995) the calculated lifetime decreased to 800 years by  
278 considering ion chemistry and assuming that the associative attachment forming SF<sub>6</sub><sup>-</sup> does not  
279 regenerate the parent molecule, thereby obtaining a lower limit for the lifetime. Reddmann *et*  
280 *al.* (2001) estimated the lifetime to be 472 yr when SF<sub>6</sub> is irreversibly destroyed purely by  
281 direct electron attachment and to be 9379 yr when SF<sub>6</sub> loss is assumed to occur only via indirect  
282 loss (via the formation of SF<sub>6</sub><sup>-</sup>) and ionization via the reactions with O<sub>2</sub><sup>+</sup> and N<sub>2</sub><sup>+</sup>. In the present  
283 study we have directly applied Troe's theory (Troe *et al.*, 2007a,b; Viggiano *et al.*, 2007) to  
284 determine the efficiency of electron attachment as a function of temperature and pressure, and



285 the branching ratio for dissociative attachment (equation E2), which we extrapolated to  
286 mesospheric conditions (Totterdill *et al.*, 2015).

287 Our estimated *partial* lifetime of SF<sub>6</sub> due to photolysis for the SF<sub>6</sub> tracer which includes all  
288 loss processes is 48,000 yr, which is considerably longer than that the 13,000 yr determined by  
289 Ravishankara *et al.* (1993) despite our Lyman- $\alpha$  cross section ( $1.37 \times 10^{-18}$  cm<sup>2</sup>, **Table 1**) being  
290 only ~22% smaller than the value the value measured by Ravishankara *et al.* ( $1.76 \times 10^{-18}$  cm<sup>2</sup>).  
291 One reason why our photolysis-related partial lifetime is longer is that WACCM includes  
292 diffusive separation, which was not described in the earlier 2-D model study. The inclusion of  
293 diffusive separation reduces sharply the abundance of SF<sub>6</sub> at high altitudes, where photolysis  
294 is most effective. Another contributing factor could be that the VUV photolysis is important  
295 only above 80 km, while in our model runs SF<sub>6</sub> is mostly destroyed by electron attachment,  
296 which results in less being transported into this upper mesospheric region. When we analyse  
297 our WACCM SF<sub>6</sub> tracer which is subject to photolysis loss only, the resulting steady-state  
298 *overall* lifetime for the last model year (2007) is 17,200 yr which is only 32% larger than the  
299 value of Ravishankara *et al.* (1993) and thus more consistent with the difference in the Lyman-  
300  $\alpha$  cross sections. Finally, if we do not include the electron scaling factor to reduce the electron  
301 density below 80 km due to negative ion formation, then the SF<sub>6</sub> lifetime decreases to 776 years  
302 (not shown), which is similar to the value obtained by Morris *et al.* (1995).

### 303 **3.3 Impact of SF<sub>6</sub> loss on mean age of stratospheric air**

304 As SF<sub>6</sub> is a chemically stable molecule in the stratosphere and troposphere, and has an almost  
305 linearly increasing tropospheric abundance, its atmospheric mixing ratio is often used to  
306 determine the mean age of stratospheric air. This is an important metric in atmospheric science  
307 as the distribution of ozone and other greenhouse gases depends significantly on the transport  
308 of air into, within, and out of the stratosphere. WACCM contains an idealized, linearly-  
309 increasing age-of-air tracer (AOA1) that provides model age values for model experiments  
310 (Garcia *et al.*, 2011).

311 Age-of-air has generally been derived from observations by treating SF<sub>6</sub> as a passive (non-  
312 reactive) tracer. The assumption is that the global loss rate is too slow to significantly affect  
313 the lifetime. This was confirmed by Garcia *et al.* (2011) when only photolysis was included.  
314 However, when loss via electron attachment is also considered, the lifetime may become short  
315 enough that this assumption is no longer valid, in which case the stratospheric mixing ratio  
316 would appear to correspond to an earlier tropospheric mixing ratio than in reality. We have



317 compared the passive WACCM SF<sub>6</sub> tracer with that subject to all loss processes, which yields  
 318 the new lifetime of 1278 yr. The difference between these two tracers indicates the error in the  
 319 derived age-of-air that would arise in the real atmosphere if SF<sub>6</sub> is assumed to be a passive  
 320 tracer. The error caused by chemical removal can be expressed as:

$$321 \quad \Delta(\text{AoA}) = \text{AoA}(\text{reactive tracer}) - \text{AoA}(\text{passive tracer}) \quad (\text{E4})$$

322 where  $\Delta(\text{AoA})$  is the difference in the age-of-air value caused by chemical loss,  $\text{AoA}(\text{reactive}$   
 323  $\text{tracer})$  is the calculated age-of-air considering the chemical removal, and  $\text{AoA}(\text{passive tracer})$   
 324 is the value obtained from a non-reactive tracer. The expression for the age-of-air at any point  
 325 in the stratosphere can be obtained from a simplified version of (E1) that is derived from a  
 326 Taylor series expansion, retaining only the linear term; then it is expressed as

$$327 \quad \text{AoA} = [(\chi_0(\text{SF}_6) - \chi(\text{SF}_6)) / r(\text{SF}_6)] \quad (\text{E5})$$

328 where  $\chi(\text{SF}_6)$  and  $\chi_0(\text{SF}_6)$  are the SF<sub>6</sub> volume mixing ratios at the actual and the reference  
 329 (tropical tropopause) points, respectively, while  $r(\text{SF}_6)$  is the rate of increase of tropospheric  
 330 SF<sub>6</sub>. In our simulations  $r(\text{SF}_6)$  is 0.29 pptv/year (**Figure 4**), which is an approximation as the  
 331 growth rate is not constant in reality. Stiller *et al.* (2012) report a value of 0.24 pptv/year based  
 332 on observations. These two simplifications will lead to deviations between WACCM and  
 333 MIPAS age data. If (E5) is substituted into (E4) then the error in age-of-air will be:

$$334 \quad \Delta(\text{AoA}) = (\chi(\text{SF}_{6, \text{passive}}) - \chi(\text{SF}_{6, \text{reactive}})) / r(\text{SF}_6) \quad (\text{E6})$$

335 This error, along with the mean age itself, was calculated from WACCM output for 2007.  
 336 **Figure 7** shows the annual mean ages determined from the WACCM simulation from 2002-  
 337 2007 using the total reactive and the inert SF<sub>6</sub> tracers and the idealized AOA1 age tracer. There  
 338 is a clear difference between the age values derived from the passive SF<sub>6</sub> and the idealized AoA  
 339 tracer. If equation (E5) is used to determine the age values there is no guarantee that the age  
 340 values derived from the two tracers will be identical; the rate was determined from the increase  
 341 of the SF<sub>6</sub> burden (0.29 pptv/year) and this was provided by the linear fit (**Figure 4**), which  
 342 can misrepresent the growth rate at any time. **Figure 7** also shows the difference between the  
 343 age values obtained from the reactive and inert SF<sub>6</sub> tracers. It can be seen that consideration of  
 344 the reactive SF<sub>6</sub> tracer does indeed affect the determined mean age values, mostly where  
 345 electron attachment dominates. The age estimates at high latitudes are most sensitive to  
 346 chemical loss because the air that reaches these locations has descended from the high altitudes



347 where SF<sub>6</sub> loss predominantly occurs. According to the MIPAS satellite observations (Stiller  
348 *et al.*, 2012; Haenel *et al.*, 2015.), the derived age value over the tropical lower stratosphere at  
349 25 km is slightly more than 3 years, while the WACCM simulations with the reactive SF<sub>6</sub> tracer  
350 predicts 3 years. Comparing **Figures 7a** and **7b**, the effect of chemical removal in this region  
351 is minor (0.01 year or 0.5% change) and therefore it does not have much impact on the inferred  
352 atmospheric transport. At the poles the effect is much more significant; the difference at 25 km  
353 between the reactive and inert SF<sub>6</sub> tracers is up to 0.55 years (9%). This means that in the  
354 troposphere-stratosphere low latitude regions the effect of chemical removal is not very  
355 significant and the error on the estimated mean age caused by the assumption of SF<sub>6</sub> being a  
356 passive tracer is not important. However, the effect of chemical removal becomes more  
357 significant at high latitudes.

358 We can also compare modelled and observed mean age values in the lower stratosphere (20  
359 km). **Figure 8** shows the mean age profiles from WACCM tracers, ER-2 observations (Hall *et*  
360 *al.*, 2009) and our analysis of MIPAS SF<sub>6</sub> satellite data at 20 km. From this it can be seen that  
361 in the tropical region the mean age values are similar between the idealized age tracer and the  
362 inert and reactive SF<sub>6</sub> tracers. This is consistent with no loss of SF<sub>6</sub> having occurred in air  
363 parcels in the deep tropics. At high latitudes there is up to 0.5 year difference in the modelled  
364 mean ages, with the reactive SF<sub>6</sub> tracer producing the oldest apparent age. The differences in  
365 mean age between the tracers is larger in the SH polar region than in the NH because the polar  
366 region is less well mixed. The tendency is very similar when we compare the WACCM mean  
367 ages to the MIPAS observations. Note that the satellite observations show more seasonal  
368 variability in the middle and high latitudes than in the tropics.

### 369 **3.4 Radiative Efficiency and Forcing**

370 To determine the radiative efficiency and global warming potential of SF<sub>6</sub>, integrated cross-  
371 sections were taken from the GEISA: 2011 Spectroscopic Database (Varanasi, 2011), the  
372 HITRAN 2012 Molecular Spectroscopic Database (Rothman *et al.*, 2012), and were also  
373 measured in this study. The literature values are presented in **Table 4** for comparison with our  
374 experimentally determined values and the full SF<sub>6</sub> spectrum obtained in this study is given in  
375 **Figure 9**. In our study the spectrometer error is ±1.0% for all experiments, and the uncertainty  
376 in the sample concentrations of SF<sub>6</sub> was calculated to be 0.7%. Spectral noise was averaged at  
377 ±5×10<sup>-21</sup> cm<sup>2</sup> molecule<sup>-1</sup> per 1 cm<sup>-1</sup> band. However, at wavenumbers <550 cm<sup>-1</sup>, towards the  
378 edge of the mid infrared where opacity of the KBr optics increases, this value was 1×10<sup>-20</sup> cm<sup>2</sup>



379 molecule<sup>-1</sup> per 1 cm<sup>-1</sup> band. The error from determining the scaling cross-section was 5%. This  
380 results in an average overall error of ±5% in the cross-sections.

381 The intensities of the main SF<sub>6</sub> absorption bands (925-955 cm<sup>-1</sup>) measured in this study are 7%  
382 greater than those reported by (Hurley, 2003), 1% greater than GEISA (Varanasi, 2011) and 1%  
383 lower than those given in HITRAN (Rothman *et al.*, 2012) (**Table 4**). Comparison of our results  
384 against Varanasi (2011) between 650 and 2000 cm<sup>-1</sup> gives an agreement within 9%. Note that  
385 these differences are within the combined error of both experiments.

386 The instantaneous and stratospheric adjusted SF<sub>6</sub> radiative efficiencies in clear and cloudy sky  
387 conditions are given in **Table 5**. These are also presented as present-day radiative forcings  
388 employing a current surface concentration of 9.3 pptv (NOAA, 2016) (see **Figure 4**). The  
389 radiative efficiency was calculated in the RFM for each month between 90°S and 90°N at  
390 latitudinal resolutions (on which the data was averaged to obtain the zonal mean vertical  
391 profile) of 1.5° and 9.0°. The tropopause used the standard WMO lapse rate definition (see  
392 Totterdill *et al.*, 2016). **Figure 10** shows the seasonal-latitudinal variation of the instantaneous  
393 clear sky radiative forcing for SF<sub>6</sub> on the high (1.5°) and low (9°) resolution grids. Employing  
394 profiles averaged over the lower resolution grid gives an average forcing within 1% of the  
395 higher resolution grid. Using only a single annually averaged global mean profile led to a 10%  
396 error in radiative forcing when compared to our monthly resolved high resolution profile,  
397 supporting the findings of Freckleton *et al.* (1998) and Totterdill *et al.* (2016).

398 A selection of experiments were carried out over a range of months and latitudes to investigate  
399 the sensitivity of the forcing calculations to the bands used. The average contributions from the  
400 main bands were compared against the calculation with the full measured spectrum. The results  
401 showed that the 580 – 640 and 925 – 955 cm<sup>-1</sup> bands contribute almost 99% to the instantaneous  
402 radiative forcing. Our forcing calculations suggest that the SF<sub>6</sub> minor bands contribute only a  
403 small amount to the final value. This means that deviations between our experimentally  
404 determined spectra and those in the literature only result in a significant change to previously  
405 published radiative forcings and efficiencies when that deviation occurs over a major band.

406 The SF<sub>6</sub> adjusted cloudy sky radiative efficiency published by the IPCC AR5 report and used  
407 to determine its GWP values is 0.57 Wm<sup>-2</sup> ppbv<sup>-1</sup> (Myhre *et al.*, 2013). This compares to the  
408 adjusted cloudy sky radiative efficiency determined in this study of 0.59 Wm<sup>-2</sup> ppbv<sup>-1</sup>. A review  
409 on radiative efficiencies and global warming potentials by Hodnebrog *et al.* (2013) provides a



410 comprehensive list of all published values for these parameters for many species including SF<sub>6</sub>.  
411 They established the range of published radiative efficiencies for SF<sub>6</sub> to be 0.59 – 0.68 Wm<sup>-2</sup>  
412 ppbv<sup>-1</sup>, with a mean value of 0.56 Wm<sup>-2</sup> ppbv<sup>-1</sup>. They also made their own revised estimate  
413 using an average of the HITRAN (Rothman *et al.*, 2012) and GEISA (Hurley, 2003; Varanasi,  
414 2011) spectral databases and found a best estimate of (0.565 ± 0.025) Wm<sup>-2</sup> ppbv<sup>-1</sup>. Their mean  
415 value for radiative efficiency is very close to that determined in this study using similar  
416 conditions (0.59 Wm<sup>-2</sup> ppbv<sup>-1</sup>).

### 417 **3.5 Global Warming Potential**

418 **Table 6** gives our estimates of the 20, 100 and 500-year GWPs based on cloudy sky adjusted  
419 radiative efficiencies of SF<sub>6</sub> compared with IPCC AR5 values (IPCC, 2013). Our 20, 100 and  
420 500-year global warming potentials for SF<sub>6</sub> are 18,000, 23,800 and 31,300 respectively. The  
421 20-year and 100-year values are 3% greater and 1% greater, respectively, than their IPCC  
422 counterparts and the 500-year GWP is 4% smaller than its AR4 counterpart (Forster *et al.*,  
423 2007). Forcing efficiencies determined in this study are somewhat higher than previously  
424 published values, which imply a higher value for GWP. However, our shorter atmospheric  
425 lifetimes would lead to a smaller GWP estimate. The trade-off between these competing effects  
426 is apparent in **Table 6**, where SF<sub>6</sub> exhibits a 20-year GWP that is slightly larger than the IPCC  
427 value, while the 500-year GWP is slightly smaller. The radiative efficiency effect is most  
428 obvious for the case of the 20-year GWP where, because the atmospheric lifetime of SF<sub>6</sub> is  
429 1278 years, the species does not have time for any significant loss to occur.

### 430 **4 Conclusions**

431 The 3D Whole Atmosphere Community Climate Model was used to simulate the SF<sub>6</sub>  
432 atmospheric distribution over the period of 1995-2007. From the concentrations and the  
433 knowledge of the electron attachment, photolysis and metal reaction rates we determined the  
434 atmospheric lifetime which shows a significant dependence on the solar cycle due to varying  
435 electron density. The mean SF<sub>6</sub> atmospheric lifetime and 1σ variation over a solar cycle were  
436 determined to be 1278 years (ranging from 1120 to 1475 years), which is different to previously  
437 reported literature values and much shorter than the widely quoted value of 3200 years. The  
438 reason is our more detailed treatment of electron attachment using a new formalism to describe  
439 both associative and dissociative attachment, and the use of a detailed model of D region ion  
440 chemistry to evaluate the partitioning of electrons and negative ions below 80 km.



441 Based on this new estimate of the SF<sub>6</sub> lifetime, we find that the derived mean age of  
442 stratospheric air from observations can be slightly affected by the atmospheric removal of SF<sub>6</sub>.  
443 In the polar region the age-of-air values differ by up to 9% when the values from inert and  
444 reactive model tracers are compared, suggesting that SF<sub>6</sub> loss does not have a large influence  
445 on the age values but that it should be included in detailed analyses.

446 We also re-investigated the radiative efficiency and global warming potential of SF<sub>6</sub>. Our  
447 radiative efficiency value reported here,  $0.59 \pm 0.045 \text{ Wm}^{-2} \text{ ppbv}^{-1}$ , is slightly higher than the  
448 IPCC AR5 estimate of  $0.57 \text{ Wm}^{-2} \text{ ppbv}^{-1}$ . The global warming potentials of SF<sub>6</sub> for 20, 100  
449 and 500 years have been determined to be 18,000, 23,800 and 31,300, respectively. We find  
450 that our revised lifetime and efficiency values somewhat cancel each other out so overall do  
451 not play a significant role in modifying the GWP estimates.

#### 452 **Acknowledgements**

453 This work was part of the MAPLE project funded by research grant NE/J008621/1 from the  
454 UK Natural Environment Research Council, which also provided a studentship for AT. The  
455 authors are also thankful to Prof Jürgen Troe for the helpful discussions related to the electron  
456 attachment to SF<sub>6</sub>.





457 **References**

- 458 Chabrilat, S. and Kockarts, G.: Simple parameterization of the absorption of the solar Lyman-  
459 alpha line, *Geophys. Res. Lett.*, 24, 2659-2662, 1997.
- 460 Dudhia, A.: Reference Forward Model V4.30: <http://www.atm.ox.ac.uk/RFM>, 2013.
- 461 Edwards, D. P.: GENLN2: The new Oxford line-by-line atmospheric transmission/radiance  
462 model, Clarendon Laboratory, Oxford, 1987.
- 463 Freckleton, R. S., Highwood, E. J., Shine, K. P., Wild, O., Law, K. S., and Sanderson, M. G.:  
464 Greenhouse gas radiative forcing: Effects of averaging and inhomogeneities in trace gas  
465 distribution, *Q. J. Roy. Meteor. Soc.*, 124, 2099-2127, 10.1002/qj.49712455014, 1998.
- 466 Forster, P., V. Ramaswamy, P. Artaxo, T. Berntsen, R. Betts, D.W. Fahey, J. Haywood, J.  
467 Lean, D.C. Lowe, G. Myhre, J. Nganga, R. Prinn, G. Raga, M. Schulz and R. Van  
468 Dorland: Changes in Atmospheric Constituents and in Radiative Forcing. *In: Climate  
469 Change 2007: The Physical Science Basis. Contribution of Working Group I to the Fourth  
470 Assessment Report of the Intergovernmental Panel on Climate Change*, Cambridge  
471 University Press, Cambridge, United Kingdom and New York, NY, USA, 2007.
- 472 Garcia, R. R., Randel, W. J., and Kinnison, D. E.: On the determination of age of air trends  
473 from atmospheric trace species, *J. Atmos. Sci.*, 68, 139-154, 2011.
- 474 Garcia, R. R., López-Puertas, M., Funke, B., Marsh, D. R., Kinnison, D. E., Smith, A. K. and  
475 González-Galindo, F.: On the distribution of CO<sub>2</sub> and CO in the mesosphere and lower  
476 thermosphere, *J. Geophys. Res.*, 119, 5700-5718, 2014.
- 477 Geller, L. S., Elkins, J. W., Lobert, J. M., Clarke, A. D., Hurst, D. F., Butler, J. H., and Myers,  
478 R. C.: Tropospheric SF<sub>6</sub>: Observed latitudinal distribution and trends, derived emissions and  
479 interhemispheric exchange time, *Geophys. Res. Lett.*, 24, 675-678, 1997.
- 480 Haedel, F.J., Stiller, G.P., von Clarmann, T., Funke, B., Eckert, E., Glatthor, N., Grabowski,  
481 U., Kellmann, S., Kiefer, M., Linden, A. and Reddman, T.: Reassessment of MIPAS age  
482 of air trends and variability, *Atmos. Chem. Phys.*, 15, 13161-13176, 2015.
- 483 Hall, T.M., and Plumb, R.A.: Age as a diagnostic of stratospheric transport. *J. Geophys. Res.*,  
484 99, 1059-1070, 1994.
- 485 Hall, T. M., Waugh, D. W., Boering, K. A., and Plumb, R. A.: Evaluation of transport in  
486 stratosphere models, *J. Geophys. Res.*, 104, 18815-18839, 1999.
- 487 Harnisch, J., and Eisenhauer, A.: Natural CF<sub>4</sub> and SF<sub>6</sub> on Earth, *Geophys. Res. Lett.*, 25, 2401-  
488 2404, 1998.



- 489 Hodnebrog, Ø., Etminan, M., Fuglestedt, J. S., Marston, G., Myhre, G., Nielsen, C. J., Shine,  
490 K. P., and Wallington, T. J.: Global warming potentials and radiative efficiencies of  
491 halocarbons and related compounds: A comprehensive review, *Rev. Geophys.*, 51, 300-378,  
492 10.1002/rog.20013, 2013.
- 493 Hurley, M. D.: GEISA : 2011 Spectroscopic Database; SF<sub>6</sub> Infrared Absorption Cross-sections,  
494 2003.
- 495 IPCC: Climate Change 2013: The Physical Science Basis. Contribution of Working Group I to  
496 the Fifth Assessment Report of the Intergovernmental Panel on Climate Change, Cambridge  
497 University Press, Cambridge, United Kingdom and New York, NY, USA, 1535 pp., 2013.
- 498 Kovács, T., Feng, W., Plane, J. M. C., Chipperfield, M. P., Nagy, T., Verronen, P. T.,  
499 Andersson, M., Newnham, D., Clilverd, M., and Marsh, D. R.: D-region ion-neutral coupled  
500 chemical model, *Geosci. Model Dev.*, (submitted), 2016.
- 501 Lamarque, J.-F., Emmons, L. K., Hess, P. G., Kinnison, D. E., Tilmes, S., Vitt, F., Heald, C.  
502 L., Holland, E. A., Lauritzen, P. H., Neu, J., Orlando, J. J., Rasch, P., and Tyndall, G.: CAM-  
503 chem: description and evaluation of interactive atmospheric chemistry in CESM., *Geosci.*  
504 *Model Dev.*, 5, 369-411, 2012.
- 505 Maiss, M., and Brenninkmeijer, C. A. M.: Atmospheric SF<sub>6</sub>, trends, sources and prospects.,  
506 *Environ. Sci. Technol.*, 32, 3077-3086, 1998.
- 507 Marsh, D. R., Mills, M. J., Kinnison, D. E., and Lamarque, J.-F.: Climate change from 1850 to  
508 2005 simulated in CESM1 (WACCM), *J. Climate*, 26, 7372-7391, 2013.
- 509 Mayer, and Kylling: Technical note: The libRadtran software package for radiative transfer  
510 calculations - description and examples of use, *Atmos. Chem. Phys.*, 5, 1855-1877, 2005.
- 511 Meredith, N. P., Horne, R. B., Isles, J. D., and Rodriguez, J. V.: Extreme relativistic electron  
512 fluxes at geosynchronous orbit: Analysis of GOES E > 2 MeV electrons, *Space Weather*,  
513 13, 170-184, 2015.
- 514 Morris, R. A., Miller, T. M., Viggiano, A. A., Paulson, J. F., Solomon, S., and Reid, G.: Effects  
515 of electron and ion reactions on atmospheric lifetimes of fully fluorinated compounds, *J.*  
516 *Geophys. Res.*, 100, 1287-1294, 1995.
- 517 Myhre, G., Shindell, D., Bréon, F.-M., Collins, W., Fuglestedt, J., Huang, J., Koch, D.,  
518 Lamarque, J.-F., Lee, D., Mendoza, B., Nakajima, T., Robock, A., Stephens, G., Takemura,  
519 T., and Zhang, H.: Anthropogenic and natural radiative forcing, Cambridge (UK), New  
520 York (USA), 2013.



- 521 NOAA Earth System Research Laboratory, Halocarbons and other atmospheric trace gases,  
522 SF<sub>6</sub> – Combined Dataset, <http://www.esrl.noaa.gov/gmd/hats/combined/SF6.html>,  
523 [Accessed 1/1/2016], 2016.
- 524 Plane, J. M. C., Feng, W., and Dawkins, E. C. M.: The mesosphere and metals, *Chem. Rev.*,  
525 115, 4497-4541, 2015.
- 526 Ravishankara, A. R., Solomon, S., Turnipseed, A. A., and Warren, R. F.: Atmospheric lifetimes  
527 of long-lived halogenated species, *Science*, 259, 194-199, 1993.
- 528 Reddman, T., Ruhnke, R., and W. Kouker, W.: Three-dimensional model simulations of SF<sub>6</sub>  
529 with mesospheric chemistry, *J. Geophys. Res.*, 106, 14,525–14,537,  
530 doi:10.1029/2000JD900700, 2001.
- 531 Rothman, L. S., Gordon, I. E., Babikov, Y., Barbe, A., Benner, D. C., Bernath, P. F., Birk, M.,  
532 Bizzocchi, L., Boudon, V., Brown, L. R., Campargue, A., Chance, K., Cohen, E. A.,  
533 Coudert, L. H., Devi, V. M., Drouin, B. J., Faytl, A., Flaud, J. M., Gamache, R. R., Harrison,  
534 J. J., Hartmann, J. M., Hill, C., Hodges, J. T., Jacquemart, D., Jolly, A., Lamouroux, J., Roy,  
535 R. J. L., Li, G., Long, D. A., Lyulin, O. M., Mackie, C. J., Massie, S. T., Mikhailenko, S.,  
536 Müller, H. S. P., Naumenko, O. V., Nikitin, A. V., Orphal, J., Perevalov, V., Perrin, A.,  
537 Polovtseva, E. R., Richard, C., Smith, M. A. H., Starikova, E., Sung, K., Tashkun, S.,  
538 Tennyson, J., Toon, G. C., Tyuterev, W. G., and Wagner, G.: The HITRAN 2012 Molecular  
539 Spectroscopic Database, *J. Quant. Spectrosc. Radiat. Transfer*, 4 - 50, 2012.
- 540 Stamnes, K., Tsay, S. C., Wiscombe, W., and Laszlo, I.: DISORT, a General-Purpose Fortran  
541 Program for Discrete-Ordinate-Method Radiative Transfer in Scattering and Emitting  
542 Layered Media: Documentation of Methodology, 2000.
- 543 Stiller, G. P., von Clarmann, T., Höpfner, M., Glatthor, N., Grabowski, U., Kellmann, S.,  
544 Kleinert, A., Linden, A., Milz, M., Reddman, T., Steck, T., Fischer, H., Funke, B., Lopez-  
545 Puertas, M., and Engel, A.: Global distribution of mean age of stratospheric air from MIPAS  
546 SF<sub>6</sub> measurements, *Atmos Chem Phys*, 8, 677–695, 2008.
- 547 Stiller, G. P., von Clarmann, T., Haanel, F., Funke, B., Glatthor, N., Grabowski, U., Kellmann,  
548 S., Kiefer, M. Linden, A., Lossow, S. and López-Puertas, M.: Observed temporal evolution  
549 of global mean age of stratospheric air for the 2002 to 2010 period, *Atmos. Chem. Phys.*,  
550 12, 3311-3331, 2012.
- 551 Tapping, K. E.: The 10.7 cm solar radio flux (F10.7), *Space Weather*, 11, 394-406, 2013.



- 552 Totterdill, A., Kovács, T., Gomez-Martin, J. C., Feng, W., and Plane, J. M. C.: Mesospheric  
553 removal of very long-lived greenhouse gases SF<sub>6</sub> and CFC-115 by metal reactions, Lyman-  
554 α photolysis, and electron attachment, *J. Phys. Chem. A*, 115, 2016-2025, 2015.
- 555 Totterdill, A., Kovács, T., Feng, W., Dhormse, S., Smith, C., Martin, J. C. G., Chipperfield,  
556 M., Forster, P., and Plane, J.: Atmospheric Lifetimes, Infrared Absorption Spectra,  
557 Radiative Forcings and Global Warming Potentials of NF<sub>3</sub> and CFC-115, *Atmos. Chem.*  
558 *Phys.*, (submitted), doi:10.5194/acp-2016-231, 2016.
- 559 Troe, J., Miller, T. M., and Viggiano, A. A.: Low-energy Electron Attachment to SF<sub>6</sub>. I. Kinetic  
560 modeling of nondissociative attachment, *J. Chem. Phys.*, 127, 244303, 2007a.
- 561 Troe, J., Miller, T. M., and Viggiano, A. A.: Low-energy electron attachment to SF<sub>6</sub>. II.  
562 Temperature and pressure dependences of dissociative attachment, *J. Chem. Phys.*, 127,  
563 244304, 2007b.
- 564 Varanasi, P. and M.D. Hurley. SF<sub>6</sub> Infrared Absorption Cross-Sections. 2011 [Accessed  
565 03/03/2015] Available from:  
566 [http://ether.ipsl.jussieu.fr/ether/pubipsl/GEISA/geisa\\_crossIR\\_frame\\_2011\\_uk.jsp](http://ether.ipsl.jussieu.fr/ether/pubipsl/GEISA/geisa_crossIR_frame_2011_uk.jsp).
- 567 Verronen, P. T., Seppälä, A., Clilverd, M. A., Rodger, C. J., Kyrölä, E., Enell, C.-F., Ulich, T.,  
568 and Turunen, E.: Diurnal variation of ozone depletion during the October-November 2003  
569 solar proton events, *J. Geophys. Res.*, 110, A09S32, 2005.
- 570 Viggiano, A. A., Miller, T. M., Friedman, J. F., and Troe, J.: Low-energy electron attachment  
571 to SF<sub>6</sub>. III. From thermal detachment to the electron affinity of SF<sub>6</sub>, *J. Chem. Phys.*, 127,  
572 244305, 2007.
- 573 Waugh, D., and Hall, T: Age of stratospheric air: Theory, observations and models, *Rev*  
574 *Geophys.*, 40, doi:10.1029/2000RG000101, 2002.
- 575



576 **Tables**

577 **Table 1.** SF<sub>6</sub> loss reactions included in WACCM.

Loss process	Rate constant	Reference and comments
Na + SF <sub>6</sub>	$k = 1.80 \times 10^{-11} \exp(-590.5/T)$	From Totterdill <i>et al.</i> , (2015) Refitted for mesospheric temperatures 215-300K.
K + SF <sub>6</sub>	$k = 13.4 \times 10^{-11} \exp(-860.6/T)$	From Totterdill <i>et al.</i> , (2015) Refitted for mesospheric temperatures 215-300K.
Electron attachment	Associative attachment: $k_{EA,ass} = k_{at} \times (k_{(SF_6^- + H)[H]} + k_{(SF_6^- + HCl)[HCl]} / (j_{PD} + k_{(SF_6^- + H)[H]} + k_{(SF_6^- + HCl)[HCl]} + k_{(SF_6^- + O_3)[O_3]} + k_{(SF_6^- + O)[O]})$ Dissociative attachment: $k_{EA,diss} = k_{at} \times \beta$ , where $\beta$ is the fraction of SF <sub>6</sub> <sup>-</sup> that dissociates into SF <sub>5</sub> <sup>-</sup> .	Totterdill <i>et al.</i> , (2015).
Photolysis	Lyman- $\alpha$ : $\sigma(121.6 \text{ nm}) = 1.37 \times 10^{-18} \text{ cm}^2$ Parameterised expression over the range of 115-180 nm, based on previous measurements.	Totterdill <i>et al.</i> , (2015).

578

579 **Table 2.** Positive and negative ions included in WACCM-SIC.

Positive ions	$O_2^+$ , $O_4^+$ , $NO^+$ , $NO^+(H_2O)$ , $O_2^+(H_2O)$ , $H^+(H_2O)$ , $H^+(H_2O)_2$ , $H^+(H_2O)_3$ , $H^+(H_2O)_4$ , $H^+(H_2O)_5$ , $H^+(H_2O)_6$ , $H_3O^+(H_2O)_2(CO_2)$ , $H_3O^+(OH)$ , $O_2^+(CO_2)$ , $H_3O^+(OH)(CO_2)$ , $H_3O^+(OH)(H_2O)$ , $O_2^+(H_2O)(CO_2)$ , $O_2^+(H_2O)_2$ , $O_2^+(N_2)$ , $NO^+(H_2O)_2$ , $H^+(H_2O)(CO_2)$ , $O^+$ , $N^+$ , $N_2^+$ , $NO^+(H_2O)_3$ , $O_4^+$ , $H^+(H_2O)_2(CO_2)$ , $H^+(H_2O)_2(N_2)$
Negative ions	$O_3^-$ , $O^-$ , $O_2^-$ , $OH^-$ , $O_2^-(H_2O)$ , $O_2^-(H_2O)_2$ , $O_4^-$ , $CO_3^-$ , $CO_3^-(H_2O)$ , $CO_4^-$ , $HCO_3^-$ , $NO_2^-$ , $NO_3^-$ , $NO_3^-(H_2O)$ , $NO_3^-(H_2O)_2$ , $NO_3^-(HNO_3)$ , $NO_3^-$ $(HNO_3)_2$ , $Cl^-$ , $ClO^-$ , $NO_2^-(H_2O)$ , $Cl^-(H_2O)$ , $Cl^-(CO_2)$ , $Cl^-(HCl)$

580

 581 **Table 3.** Partial (reactions with electrons, photolysis, and metals (K, Na)) and total atmospheric  
 582 lifetimes (years) of  $SF_6$  from different studies. Numbers in parentheses show relative  
 583 percentage contribution of loss due to the different processes.

Study	Lifetime / years			
	Photolysis	Electron attachment	Total	Model dimensions
Ravishankara <i>et al.</i> (1993)	13,000 (24%)	4210 (76%)	3200	2D
Morris <i>et al.</i> (1995)	N/A	N/A	800	2D
This work	48,000 (2.6%)	1339 (97.4%)	1278	3D

584



585 **Table 4.** Integrated absorption cross-sections for SF<sub>6</sub> measured in this work and ratios with  
 586 values obtained by Hurley (2003), Varanasi (2001) and HITRAN (Rothman *et al.*, 2012).

Band limits (cm <sup>-1</sup> )	Integrated cross-section (10 <sup>-16</sup> cm <sup>2</sup> molec <sup>-1</sup> cm <sup>-1</sup> )	Ratio of integrated cross-sections in this work to previous studies		
		Hurley (2003)	Varanasi (2001)	HITRAN
925 - 955	2.02	1.07	1.01	0.99
650 - 2000	2.40	-	1.09	-

587

588 **Table 5.** Calculated instantaneous and stratospheric adjusted radiative forcings and radiative  
 589 efficiencies of SF<sub>6</sub> in clear and all-sky conditions<sup>a</sup>.

	Instantaneous		Stratospheric adjusted	
	Clear	All-sky	Clear	All-sky
Radiative forcing (mWm <sup>-2</sup> )	76.43	48.91	81.81	56.01
Radiative efficiency (Wm <sup>-2</sup> ppbv <sup>-1</sup> )	0.77	0.50	0.85	0.59

590 a. Based on present day atmospheric SF<sub>6</sub> surface concentration of 9.3 pptv.

591 **Table 6.** Comparison of 20, 100 and 500-year global warming potentials for SF<sub>6</sub> from this work  
 592 with values from IPCC (2013).

	Global Warming Potential		
	GWP <sub>20</sub>	GWP <sub>100</sub>	GWP <sub>500</sub>
This work <sup>a</sup>	18000	23700	31300
IPCC (2013) <sup>b</sup>	17500	23500	32600 <sup>c</sup>
Difference (%) (This work – IPCC)	+3%	+1%	-4%

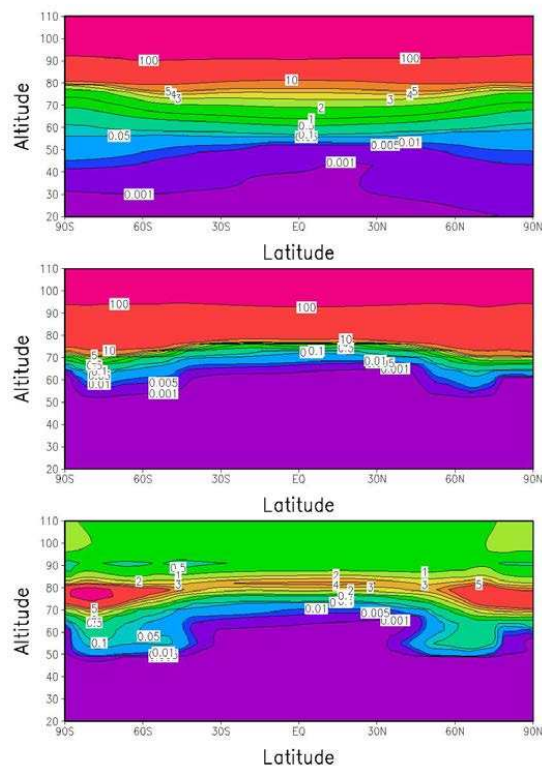
593 <sup>a</sup> Based on our atmospheric lifetime of 1278 yrs and RE of 0.59 Wm<sup>-2</sup> ppbv<sup>-1</sup>.

594 <sup>b</sup> Based on an atmospheric lifetime of 3200 yrs and RE of 0.57 Wm<sup>-2</sup> ppbv<sup>-1</sup>.

595 <sup>c</sup> Based on an atmospheric lifetime of 3200 yrs and RE of 0.52 Wm<sup>-2</sup> ppbv<sup>-1</sup> from IPCC AR4  
 596 (Forster *et al.*, 2007).



597 **Figures**



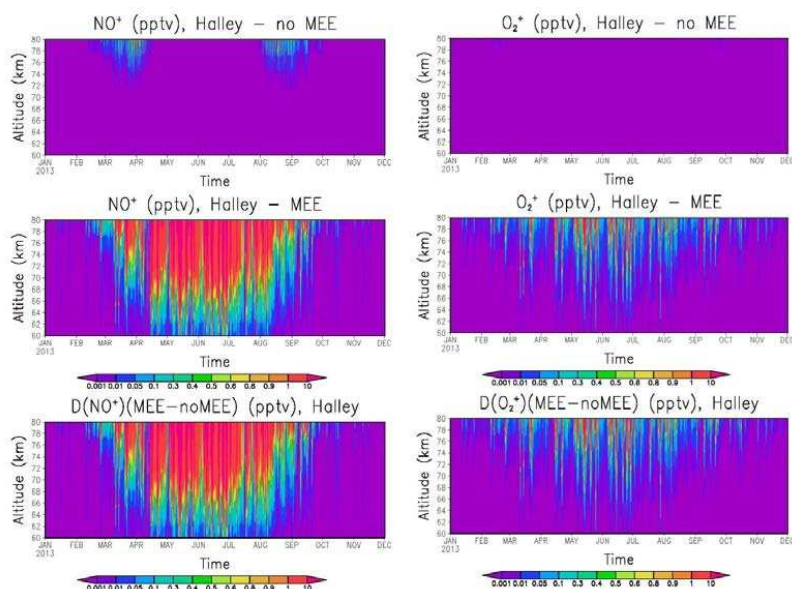
598

599 **Figure 1.** Top: annual average electron concentration for 2013 from the standard WACCM  
600 model (in  $10^2$  electrons  $\text{cm}^{-3}$ ). Middle: annual average electron concentration for 2013 from  
601 WACCM-SIC model (in  $10^2$  electrons  $\text{cm}^{-3}$ ). Bottom: annually averaged electron scaling factor  
602 for 2013.





603

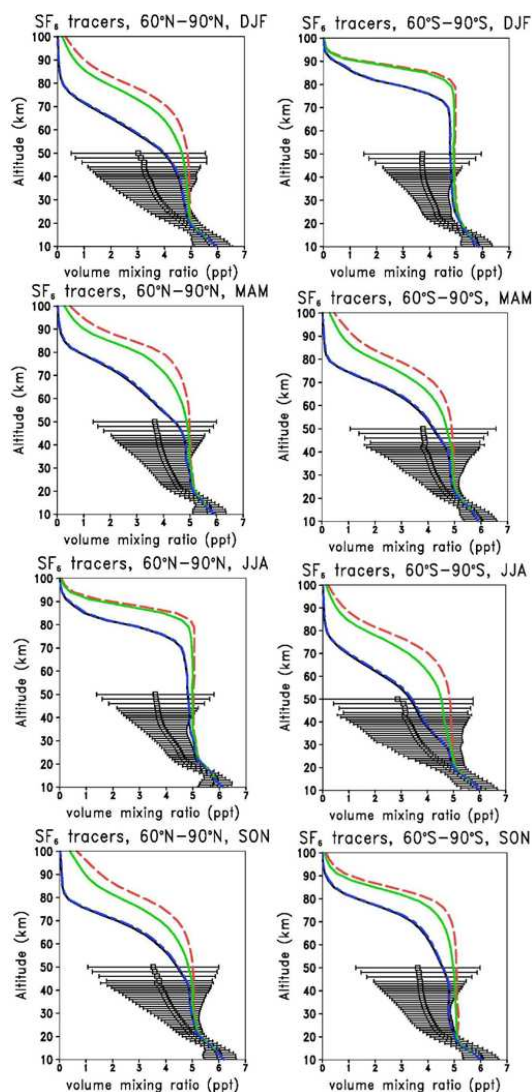


604

605 **Figure 2.** Time series of volume mixing ratio profiles (pptv) of  $\text{NO}^+$  (left panels) and  $\text{O}_2^+$  (right  
606 panels) above Halley ( $76^\circ\text{S}$ ) from two WACCM-SIC simulations. Top panels show the values  
607 obtained from the model run without medium energy electrons; the middle panels show the run  
608 with medium energy electrons; and the bottom panels show the absolute differences between  
609 the two model runs.



610

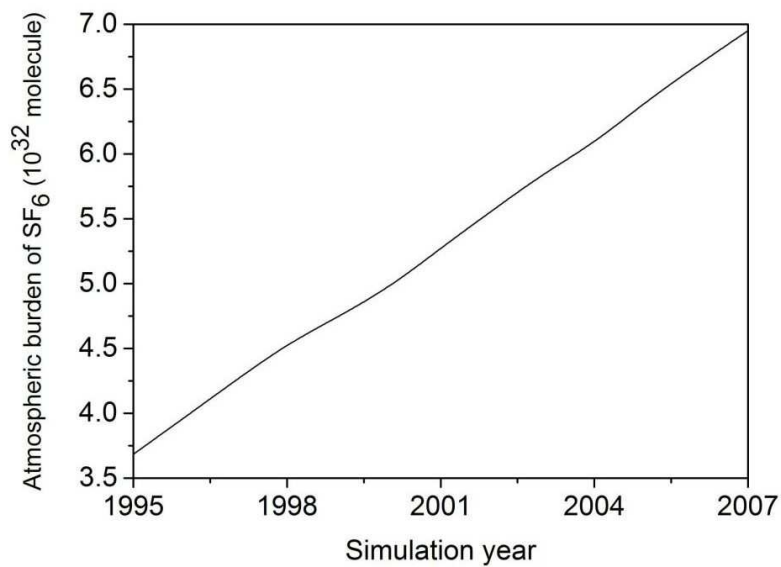


611

612 **Figure 3.** Annual volume mixing ratios (pptv) of the different SF<sub>6</sub> tracers for the polar regions  
613 (60°N – 90°N and 60°S – 90°S latitudes) in 2007 as a function of altitude for MIPAS satellite  
614 observed SF<sub>6</sub> (black symbols with standard deviations for  $\pm 1\sigma$ ) (Stiller *et al.*, 2012), the total  
615 WACCM-SF<sub>6</sub> (blue solid line), the photolysis WACCM-SF<sub>6</sub> tracer (green solid line) and the  
616 inert WACCM SF<sub>6</sub> tracer (red dashed line).



617

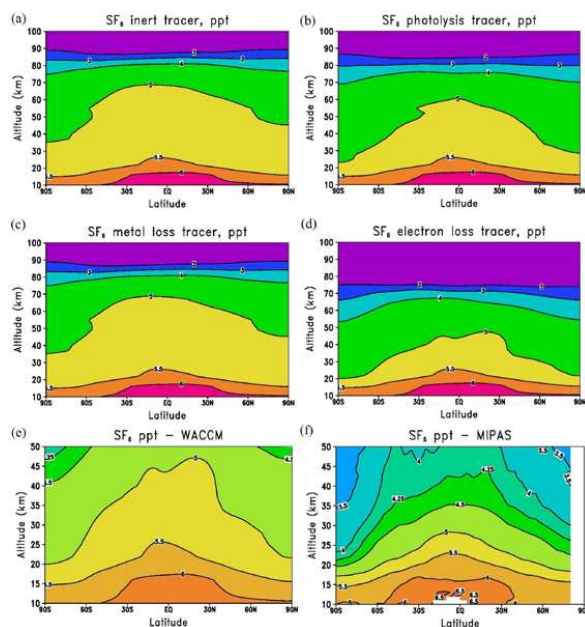


618

619 **Figure 4.** Variation of the total annual atmospheric burden of SF<sub>6</sub> during the simulation from

620 1995 to 2007. According to this the emission rate (slope) was determined to be  $6.5 \times 10^{-3}$

621 Tg/year, corresponding to 0.29 pptv/year.

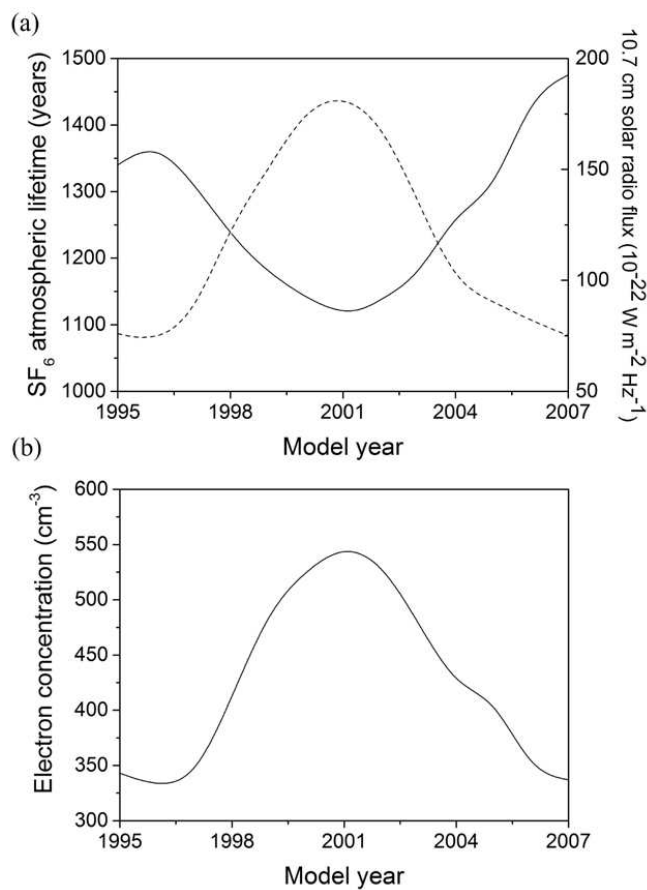


622

623 **Figure 5.** Annual zonal mean latitude-height volume mixing ratios (pptv) of the different  
624 WACCM SF<sub>6</sub> tracers in 2007: (a) inert SF<sub>6</sub> tracer; (b) SF<sub>6</sub> tracer removed by photolysis only;  
625 (c) SF<sub>6</sub> tracer removed by mesospheric metals only; (d) SF<sub>6</sub> tracer removed by electron  
626 attachment only; and (e) total reactive SF<sub>6</sub>. Panel (f) shows the SF<sub>6</sub> volume mixing ratio for  
627 2007 from MIPAS observations. Note the different altitude ranges for panels (a)-(d) and (e)-  
628 (f).

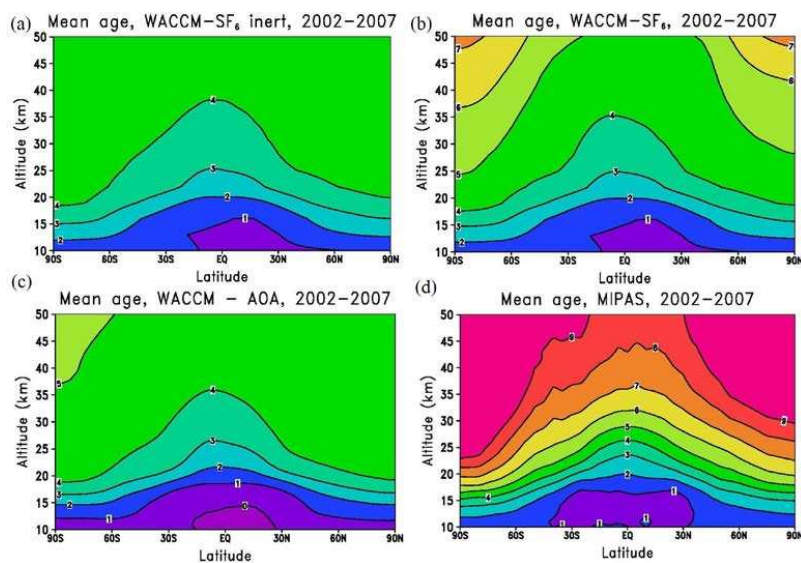


629



630

631 **Figure 6.** (a) Variation in atmospheric lifetime of SF<sub>6</sub> (solid line) and 10.7 cm solar radio flux  
632 (dashed line) during the WACCM simulation. (b) Variation of the WACCM electron  
633 concentration (cm<sup>-3</sup>) at 80 km, averaged over polar latitudes (60°N – 90°N and 60°S – 90°S).

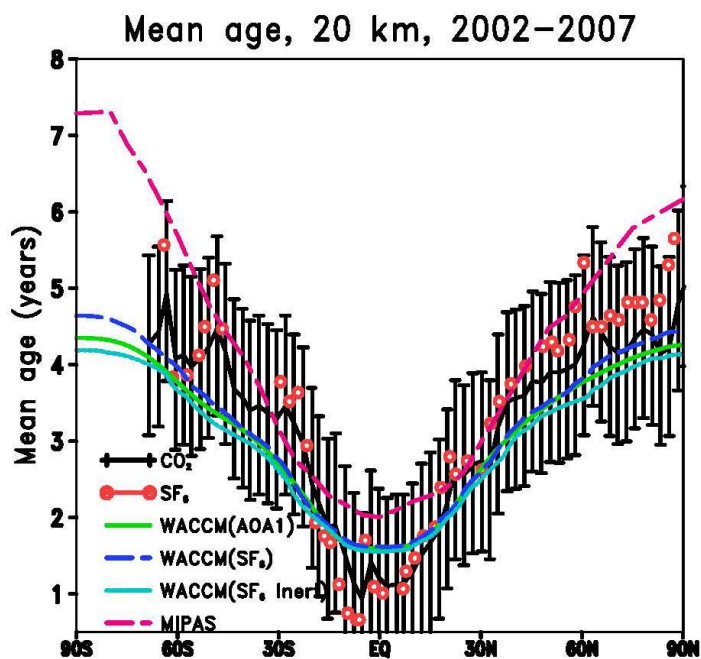


634

635 **Figure 7.** Annual mean age of stratospheric air (years) for the period of 2002–2007 determined  
636 from a WACCM simulation using: (a) the inert SF<sub>6</sub> tracer; (b) the total reactive SF<sub>6</sub> tracer; (c)  
637 the idealized AOA1 tracer. Panel (d) shows the age values derived for the same period from  
638 our analysis of MIPAS SF<sub>6</sub> observations.



639



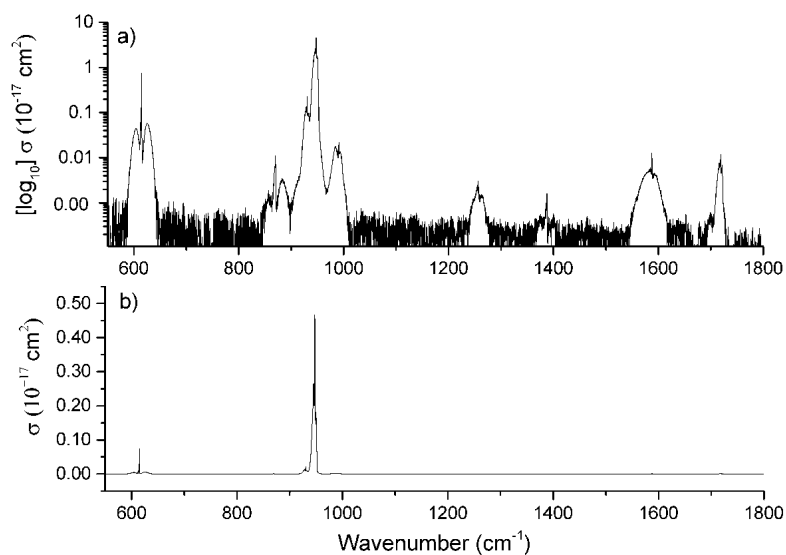
640

641 **Figure 8.** Mean age values at 20 km altitude derived from MIPAS satellite (dashed magenta  
642 line) and ER-2 aircraft observations (SF<sub>6</sub> red open circles, CO<sub>2</sub> black crosses) (Hall *et al.*,  
643 1999). The error bars apply to the age derived from the ER-2 observations. Also shown is the  
644 mean age derived from WACCM tracers: reactive SF<sub>6</sub> (dashed blue line), passive SF<sub>6</sub> (light  
645 blue line) and AOA tracer (solid green line).



646

647

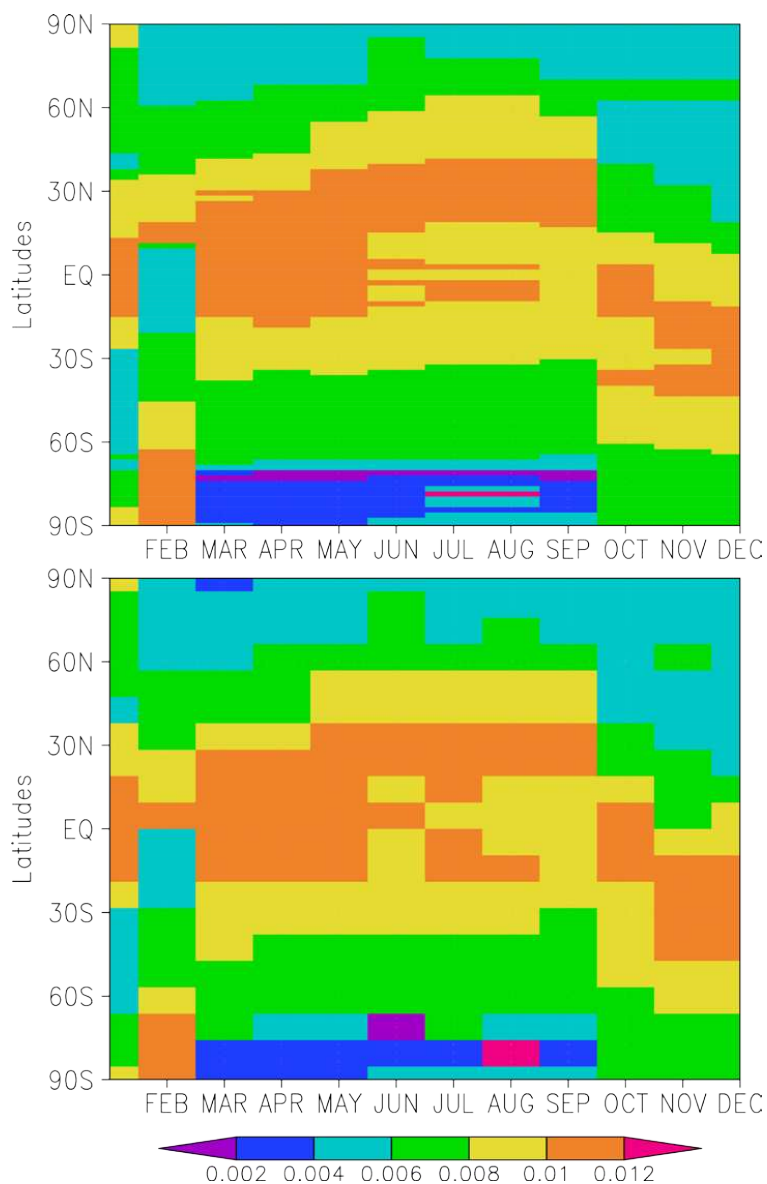


648

649

650 **Figure 9.** Infrared absorption spectrum of SF<sub>6</sub> at ~295 K on (a) a logarithmic y axis and (b) a  
651 linear y axis. The logarithmic scale in panel (a) highlights the relative positions of the minor  
652 bands.





653

654 **Figure 10.** Latitude-time plots for instantaneous radiative forcing ( $\text{Wm}^{-2}$ ) by  $\text{SF}_6$  as a function  
655 of latitude and month at (a) high latitude resolution ( $1.5^\circ$  spacing) and (b) low latitude  
656 resolution ( $9^\circ$  spacing).